University of Auckland Research Repository, ResearchSpace

Version

This is the Accepted Manuscript version. This version is defined in the NISO recommended practice RP-8-2008 http://www.niso.org/publications/rp/

Suggested Reference

Copyright

An Active RFID Tag-enabled Locating Approach with Multipath Effect Elimination in AGV

Shaoping Lu, Chen Xu, and Ray Y. Zhong, *Member, IEEE*

Abstract— **Automated guided vehicles (AGVs) have been largely used in manufacturing and supply chain management. With the development of Auto-ID technologies like radio frequency identification (RFID), AGVs' positioning could be enhanced. This paper demonstrates on using magnetic field lines in the AGVs for precise coverage locating based on the errors suppression positioning method. Dolph-Chebyshev antenna array is used to enable AGVs with more precise location implementation. It is observed that the far-field active RFID system positioning accuracy is higher, the movement is more stable and the fluctuating rate is smaller.**

Note to Practitioners— **This paper was motivated by real-life problems when companies are going to implement automation with automated guided vehicles (AGVs). By using the radio frequency identification (RFID) technology, a more precise locating approach is proposed. This approach uses active RFID tags for localization. Dolph-Chebyshev antenna array is used in this system to enable AGV with more precise location implementation by making full use the multipath effect elimination method.**

Index Terms—**Active RFID, AGV, Magnetic Field Lines, Positioning.**

I. INTRODUCTION

T HE AUTOMATION in manufacturing and supply chain management requires large number of automated guided vehicles (AGVs) for handling the materials so that the smart warehouse or factories could be enabled [1, 2]. For example, many large companies like DHL, Walmart, and Amazon are using AGVs to facilitate their goods delivery and logistics operations [3]. However, most of the applications are used fixed lanes such as rail bound approach that is usually with high cost and low flexibility since the rails are based on steels and it is difficult to reconfigure when the warehouse layout is going to be changed [4, 5].

With the development of Auto-ID technologies like radio frequency identification (RFID), which has been widely used in industrial applications in terms of item tracking, logistics tracing, and supply chain visibility [6-12]. The advantages of

RFID such as non-contact sensing, anti-dust-pollution, and multi-identification capability have attracted great myriad of attentions from both industrial and academic fields [13]. Currently, RFID has been used for localization [14]. However, most of the localization systems are based on passive tags which is limited in reading distances when implementing in real-life environments where complex materials may be comprised such as metal and humid substances [15, 16]. In order to enhance the reading distances and accuracy, active RFID tags are used for localization systems [17].

This paper introduces an active RFID tag-enabled locating method for AGV system for warehouse or manufacturing factories. This system uses magnetic field lines for precise coverage locating based on the errors suppression positioning method. Dolph-Chebyshev antenna array is used to enable AGV with more precise location implementation.

The rest of this paper is organized as follows. Section 2 gives some briefly definitions. Section 3 presents the analysis of reflection influences on signal suppressions from theoretical aspect. Section 4 illustrates the system design and implementation from practical aspect. Simulation results and physical testing in a lab are presented. Section 5 concludes this paper by giving our contributions and future work.

II. DEFINITIONS

"Errors Suppression Positioning Method" uses the measured value of the signal intensity, which is a field line equation corresponding to the directional function. It is able to solve more than three field line equations to obtain the location of an object [18]. The directional function indicates the radiation performance of an antenna in different directions since different antennas have different directional functions. But once the physical parameters of an antenna are determined, the directional function is fixed. Friis equation or radar equation has the directional function factors [19]. For example, the Friis equation describes the matching power received by the far-field receiving antenna:

$$P_{re}(\theta,\varphi) = \left[\frac{\lambda}{4\pi r}\right]^2 G_1 G_2 F_1^2(\theta,\varphi) F_2^2(\theta,\varphi) P_{in} \qquad (1)$$

As is shown in formula 1, the signal strength of far-field

Shaoping Lu is with the Department of Transport and Logistics, Shenzhen University, Shenzhen, China (e-mail: szlusp@163.com)

Chen Xu is with the Institute of Intelligent Computing Science, Shenzhen University, Shenzhen, China (e-mail: xuchen@szu.edu.cn).

Ray Y. Zhong is with the Department of Mechanical Engineering, The University of Auckland, New Zealand (e-mail: zhongzry@gmail.com).

receiving antenna, not only relates to the distance, but also relates to the wavelength, the antenna directional function and input power etc.

$$P_R = \frac{P_T}{r^n} \tag{2}$$

The above formula (2) represents the path loss model which made a great simplification of the Friis transmission equation, which does not consider the effects of antenna, instead of using transmission factor n as the effects of environment. The transmission factor depends mainly on the experiment, and obtained by experience [20]. There are many factors affected the system error. According to the different classification methods, it can be divided into theoretical errors and measurement errors, steady-state errors and disturbance errors etc [21].

It is assumed that the received signal strength value (measured) is E'_{rssi}, the theoretically received signal strength is E_{rssi}, the error produced by system is ΔE, then:

$$E_{rssi} = E'_{rssi} \pm \Delta E \tag{3}$$

Where

$$\Delta E = \sum \Delta E_t + \sum \Delta E_m \tag{4}$$

(4) includes the theoretical error $\sum \Delta E_t$ and the measurement error $\sum \Delta E_m$. If the error $\sum \Delta E_t$ and $\sum \Delta E_m$ could be suppressed, it will greatly improve the positioning accuracy.

Fig. 1 presents a canonical representation reference to the ten path model of reflection in indoor environment. Considering the signal energy would decay after each reflection, the ten path model ignored the reflection reflected more than three times [22]. The reflected signals arrive at the receiving point had phase difference due to the wave path difference, resulted in irregular overlapping, which makes the signal calculation to be very complex.
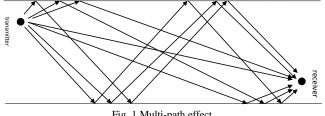

Fig. 1 Multi-path effect

Once the positions of receiving antenna and transmitting antenna are determined, various reflection signals are described by ray tracing method of signal transmission. If the influence of the main reflection could be eliminated, multiple reflection effect of the other could be reduced too. According to the current standards of measurement, 2.45GHz (2400-2483.5MHz) and 915MHz (American frequency range 902-928MHz), their impacts on the frequency reach 3.4% and 2.84% respectively, and the influence of the received signal strength reached 6.93% and 5.76% respectively [23]. Such errors doubtless have great impact for the accurate positioning of the AGV guidance. The electromagnetic field of external environment changing, especially the similar frequency electromagnetic wave will also have impact on the system. Such as the passive location system, the signal strength reflected by tag and received by reader antenna primarily depends on the signal strength. The tag is able to received, if in the same environment, there is an antenna system of similar frequency were covering this tag [24]. The energy that the tag received may be greater than the condition that only one antenna coverage, the backscatter signal intensity may deviate from its theoretical value.

Through the above analyses, "Errors Suppression Positioning Method" maybe reasonable for enhancing the AGVs locating system. An orientation and guiding system have been proposed in this paper to examine the validity. This system is composed by vehicle-mounted Dolph-Chebyshev array antenna. A group of four Dolph-Chebyshev array antennas and flat reflectors are fixed on the ground.

III. ANALYSIS OF ERRORS SUPPRESSION POSITIONING METHOD

The far-field active RFID system to the electromagnetic field is radiation field. It uses active tags. Tag comes with a battery for powering tag chip and antenna system, which ensures that the chip circuit work and initiatively emit modulated radio waves. The aforementioned "Errors Suppression Positioning Method" presents the path loss model based on analyzing received signal strength indication (RSSI) overlooked the directivity of antenna and indoor environment influence factors such as complex multi-path effect. It would naturally cause errors. Thus, it is necessary to eliminate the errors to ensure the normal operation of the AGV guidance and location.

A. Radiation Function and Pattern

1) Friis Transmission Equation

For active REID system, its Friis transport equation can be expressed as:

$$P_{re}(\theta,\varphi) = \left[\frac{\lambda}{4\pi r}\right]^2 G_1 G_2 F_R^{\ 2}(\theta,\varphi) F_S^{\ 2}(\theta,\varphi) P_{in} \tag{5}$$

$P_{re}(\theta,\varphi)$ is the power matching of the receiving antenna. That presents the RSSI that is the reader received from the tag. P_{in} is the electromagnetic wave power emitted by the tag. G_1 and $F_S(\theta,\varphi)$ are the active tag antenna gain function and normalized directional function respectively. G_2 and $F_R(\theta,\varphi)$ are the reader antenna gain function and normalized directional function respectively. λ is the wavelength of transmission of electromagnetic wave. r is the distance between reader device and tag. Once the transmitting and receiving antennas are determined, G_1, G_2 and the directional function $F_S(\theta,\varphi)$、 $F_R(\theta,\varphi)$ will be determined. $P_{re}(\theta,\varphi)$ can be measured, then we can get a field strength contour plane equation contains three variables (θ,φ,r).

When the main direction of the antennas for readers and tags are completely aligned, $F_S(\theta,\varphi) = F_R(\theta,\varphi) = 1$, (5) can be simplified as:

$$P_{re}(\theta,\varphi) = \left[\frac{\lambda}{4\pi r}\right]^2 G_1 G_2 P_{in} \tag{6}$$

Formula (6) is the foundation of path loss model. But in the process of positioning, it is hard to get the main direction of antennas. Isotropic omnidirectional antenna does not exist too. Therefore, the directional function is an important factor to the RSSI of formula (5). In (5), wavelength λ will change as the frequency hopping, which will influence the value of RSSI. P_{in} will change as the tag battery consumption changing, which also influences the value of RSSI.

2) Directional Function and Beam Angle of Antenna

Directional function also called beam function expresses the characteristics of the antenna radiation direct. Let the antenna as the radiation source, the field strength is different in different direction expressed as $f(\theta,\varphi)$. Where, θ is the angle in vertical direction, φ is the angle in horizontal direction. Power directional function was expressed as $f^2(\theta,\varphi)$. The normalized directional function of field strength is:

$$F(\theta,\varphi) = \frac{|f(\theta,\varphi)|}{Max|f(\theta,\varphi)|} \tag{7}$$

The graph of directional function is called directional diagram or beam pattern. The direction diagram of the antenna was composed by several beams, the maximum radiation direction beam is the main beam. Features of the antenna can be expressed by the width of the main beam, side beam level etc. The width of the main beam is HPBW (Half-power Beam Width), which is the intersection angle between two points whose power are equal to the maximum power on the main beam. FNBW is the maximum width of beam. The radiation power can be ignored compared with the maximum direction, as is shown in Fig. 2.
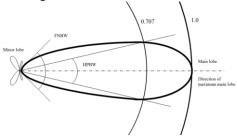

Fig. 2 Typical antenna beam pattern

With different antenna arrays, different directional diagram could be obtained. For example, the directional function of dipole is:

$$F(\theta,\varphi) = \sin\theta \tag{8}$$

The HPBW of dipole is 90°, the FNBW is 180°. For the feed dipole, directional function is:

$$F(\theta,\varphi) = \frac{\cos\left(\frac{\beta L\cos\theta}{2}\right) - \cos\left(\frac{\beta L}{2}\right)}{\sin\theta} \tag{9}$$

When $L = \lambda/2$, it is usually called "half-wave antenna", $\beta L = \pi$ ($\beta = \frac{2\pi}{\lambda}$ is the phase constant), half wave antenna directional function can be obtained:

$$F(\theta,\varphi) = \frac{\cos\left(\frac{\pi}{2}\cos\theta\right)}{\sin\theta} \tag{10}$$

Let $F(\theta,\varphi) = 0.707$, HPBW is $78.12°$. Let $F(\theta,\varphi) = 0$, FNBW is $179.82°$. When $L = \lambda$, it is usually called "full-wave antenna". When $\beta L = 2\pi$, directional function of full-wave oscillator is:

$$F(\theta,\varphi) = \frac{\cos(\pi\cos\theta) + 1}{\sin\theta} \tag{11}$$

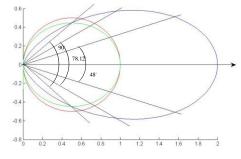In the same way HPBW is $48°$, and the FNBW is $166.68°$.

Fig. 3 Directional diagram of several typical antenna

Fig. 3 shows the directional diagram and the HPBW of dipole, half-wave antenna and full-wave antenna. Although the HPBW can be changed by selecting different antenna, the influence to FNBW is small. According to the multiplication principle of antenna:

$$F(\theta,\varphi) = g(\theta,\varphi) f(\theta,\varphi) \tag{12}$$

$g(\theta,\varphi)$ is the directional function of a single unit of antenna array and $f(\theta,\varphi)$ is the factor of antenna array. In order to get a desired directional function and beam width, different antenna array can be designed by selecting different array factor of changing the composition of antenna array. Fig. 4 shows the directional function of coaxial half-wave dipole and full-wave dipole in different spacing. As shown in Fig. 4, changing the length of antenna and distance between antennas have great influence on the directional diagram. The gain of directional diagram increases as the length of antenna increasing and the beam width decreases as the distance between antennas increasing. For example, if the distance between coaxial half-wave dipole antennas is a wavelength, the main beam width is 37.62° and the FNBW can reach 106.02°.
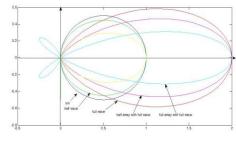

Fig. 4 Directional diagram of antenna array

B. Influence of Reflection and Analysis of Suppression

1) Analysis of Vertical Reflection and Restraining Measures

In indoor condition, the vertical reflection is mainly caused by ground and ceiling, which is the main factor of multiple reflection and influencing the strength of received signal.
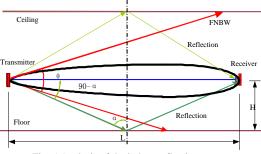

Fig. 5 Analysis of the indoor reflection sources

Fig. 5 is an analysis of the indoor reflection sources. The black curve shows the directional diagram of antenna in vertical direction. The angle between the two red half-lines is the FNBW. The green half-line shows the reflected ray from ground. Light green half-line shows reflected ray from ceiling. Let the height of the sending and receiving antenna is H, when the distance between emission source and the receiving points is L, take the reflection from the ground for example, according to the Snell's law, the angle of incidence is equal to the angle of reflection. When the reflection point is on the right side of the midpoint L/2, the reflected signals cannot reach to the receiver. If the reflection point is on the left side of the midpoint, the reflection will affect the receiver signal strength. In a summary, if FNBW is small enough, the radiation range can't reach the midpoint of the left

The FNBW of the main beam is θ. When $\theta/2$ is smaller than the complement angle of the incident angle which is $90° - \alpha$, the reflection of the electromagnetic wave cannot influence on the received signal. Due to $\tan\alpha = L/(2H)$, the prerequisite that doesn't affect the received signal is

$$\theta < 2\left[\frac{\pi}{2} - \arctan\left(\frac{L}{2H}\right)\right] \tag{13}$$

According to the maximum working range of general active RFID, assuming the maximum working distance is $L = 20m$, antenna height is $H = 2m$. When $\theta < 22.6°$ the influence from the ground reflection can be effectively suppressed.

Therefore, in this paper, considering the design of an antenna array, of which FNBW is small enough to meet the above requirements. Dolph-Chebyshev distribution is used. Take the five source array within distance $\lambda/2$ for example, the side beam level is $-20dB$, the relative amplitude of the optimal pattern is {1,1.6,1.9,1.6,1}, its HPBW is 27°. It is narrower than the HPBW of binomial distribution.

From the above analysis, when the amplitude to the array ends taper change hours (binomial distribution), side beam is to weaken until disappear. When the amplitude from two ends to the center of the array tapered to zero (marginal distribution), side beam increases to equal as main beam. Therefore, it could be observed that the side beam level is closely related to the mutation of the amplitude distribution in the array at the edge.

The discontinuity of amplitude distribution can lead to huge side beam. And the zero distribution on the edge can minify the discontinuity so that the side beam amplitude will be minimized. Dolph-Chebyshev array guarantees the minimization of HPBW and the FNBW. The field strength value of the antenna arrays have different formulas according to the parity of point sources:

$$\begin{cases} E_{n_e} = 2\sum_{k=0}^{k=n/2-1} A_k \cos\left(\frac{2k+1}{2}\psi\right) & \text{when } n \text{ is even} \\ E_{n_e} = 2\sum_{k=0}^{k=(n-1)/2} A_k \cos\left(\frac{2k}{2}\psi\right) & \text{when } n \text{ is odd} \end{cases} \tag{14}$$

n is the number of point sources. $\psi = \frac{2\pi d}{\lambda}\sin\theta$. d is the antenna array spacing. $A_o, A_1, A_2 \ldots$ is symmetry in the center of the point source. Combining with the double angle formula and triple angle formula to simplify $\cos m\frac{\psi}{2}$, we can get:

$$\cos m\frac{\psi}{2} = \cos^m\frac{\psi}{2} - \frac{m(m-1)}{2!}\cos^{m-2}\frac{\psi}{2}\sin^2\frac{\psi}{2} + \frac{m(m-1)(m-2)(m-3)}{4!}\cos^{m-4}\frac{\psi}{2}\sin^4\frac{\psi}{2} - \cdots$$

let $x = \cos\frac{\psi}{2}$, Chebyshev polynomial can be simplified as:

$$T_m(x) = \cos m\frac{\psi}{2} \tag{15}$$

Dolph-Chebyshev antenna array, according to the particular side beam level under the minimum request, uniquely determine the coefficient of beam pattern series. Power of polynomial is always less than source number n. In order to determine the antenna source amount of Dolph-Chebyshev array and ideal sidebeam level value, Table 1, 2, and 3 show the results by letting the distance d between the antennas is $\lambda/2$. The number of antenna array are 5, 6, 7 and 8. Side beam level are 12dB, 16dB, 18dB, 20dB, 26dB, 32dB and 38dB.

Table. 1 HPBW

Amount	SLL=12	SLL=16	SLL=18	SLL=20	SLL=26	SLL=32	SLL=38
N=5	9.96	10.73	11.05	11.39	12.14	12.71	13.11
N=6	8.15	8.84	9.16	9.44	10.21	10.82	11.28
N=7	6.89	7.49	7.78	8.07	8.78	9.35	9.84
N=8	5.95	6.50	6.77	7.00	7.67	8.24	8.70

Table. 2 FNBW

Amount	SLL=12	SLL=16	SLL=18	SLL=20	SLL=26	SLL=32	SLL=38
N=5	22.52	25.38	26.76	28.07	31.80	34.89	37.30
N=6	19.31	20.57	21.72	22.92	26.18	29.05	31.46
N=7	15.18	17.25	18.28	19.31	22.17	24.81	27.04
N=8	12.70	14.84	15.76	16.62	19.25	21.60	23.66

Table. 3 Influence coefficient of side beam

Amount	SLL=12	SLL=16	SLL=18	SLL=20	SLL=26	SLL=32	SLL=38
N=5	0.19	0.12	0.09	0.07	0.03	0.03	0.03
N=6	0.21	0.13	0.10	0.08	0.04	0.03	0.03
N=7	0.22	0.14	0.11	0.09	0.04	0.03	0.03
N=8	0.19	0.14	0.11	0.09	0.04	0.03	0.03

Table. 1 and 2 express HPBWs and FNBWs of Dolph-Chebyshev antenna arrays. It could be found that with the increasing of SLL, the cumulative HPBW values will increase. But with the increasing number of antennas, for the same SLL, HPBW reduces. Therefore, in order to get antenna array within small beam angle, eight elements Dolph-Chebyshev antenna array is the most economical choice. For the determined SSL and number of antenna unit, changing the spacing of antenna unit, Table. 4 and Fig. 6 could be obtained.

Table. 4 The influence from antenna spacing to HPBW and FNBW (unit: °)

$S(\lambda)$	0.4	0.5	0.6	0.7	0.8	0.9		1.1	1.2	1.3
FNBW	26.76	21.54	15.76	13.06	11.17	10.54	9.95	8.42	8.20	7.17
HPBW	8.41	6.77	5.66	4.86	4.25	3.79	3.42	3.11	2.84	2.62

(a) $S = 0.5\lambda$ (b) $S = 0.8\lambda$
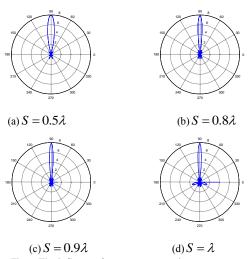
(c) $S = 0.9\lambda$ (d) $S = \lambda$

Fig. 6 The influence from antenna spacing to pattern

In Table. 4, it can be seen that with the increasing of S, HPBW and FNBW will reduce. As shown in Fig. 6, the number of side beam increases along with the augment of S. $S = 0.9\lambda$ meets the requested side beam extreme. When $S = \lambda$, side-beam amplitude is greater than 10% of the main beam amplitude. Thus antenna spacing is determined as 0.9λ, then the FNBW is 21°, meeting the requirement that the incident angle should be less than 22.6° of vertical reflection.

2) Analysis of Horizontal Reflection and Restraining Measures

According to the characteristics of AGV's workplace, there are walls around in the warehouse, if the horizontal omnidirectional antenna is placed in the edge of the workplace, such as close to the wall, as shown in Fig. 7(a), the electromagnetic field radiated from the antenna would certainly be influenced by the multipath effect. Regards to this, the reflector is widely used to change the directional diagram of radiation unit. If we placed a certain size of planar reflector at a side of the antenna in a proper distance, as shown in Fig. 7(b), the electromagnetic field signal reflected by the plane, forming an oval electromagnetic wire on the other side of the antenna. Thereby the backward radiation of antenna can be restricted, which is also the radiation from the antenna to the wall. Then the reflection effect in the horizontal direction can be effectively inhibited.
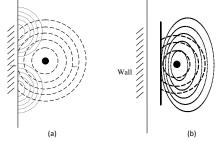

(a) (b)

Fig. 7 Radiation fields of with and without flat reflector

The errors suppression method in the horizontal direction is to use an flat reflector antenna to eliminate backward radiation. The distance between antennas and flat reflectors could influence on power beam width. By using image method, it is easy to deal with the problem of the antenna which is at a distance of S apart from the ideal infinite conductive flat reflector. In this method, the mirror image which is $2S$ apart from the original antenna is used to replace the reflector. If the original is $\lambda/2$ dipole antenna, assuming reflector is lossless, then the field gain of $\lambda/2$ dipole antenna is at a distance of S. The infinite ideal conductive flat reflector is:

$$G_f(\phi) = 2\sqrt{\frac{R_{11} + R_L}{R_{11} + R_L - R_{12}}} \left| \sin\left(S_r \cos(\phi)\right) \right| \tag{16}$$

$S_r = 2\pi S/\lambda$. R_L is the loss resistance of the dipole. G_f is relative to the free space $\lambda/2$ antenna with the same input power. Changing S, Fig. 8 could be obtained.

(a) (b)

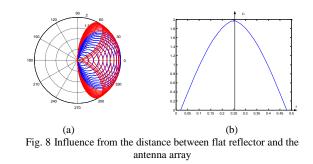Fig. 8 Influence from the distance between flat reflector and the antenna array

Fig. 8 (a) shows the field strength of changing the S_r in the flat reflector formula. The blue area shows the changing of S_r in $0.04\pi \sim 0.52\pi$. Field strength figure changes from round to oval. The red area shows that the changing of S_r in $0.52\pi \sim \pi$. Field strength figure changes from oval into irregular geometry

and two side beam appears. Fig 8 (b) presents the radiation strength along with the changing of S. It is observed that, with the increasing of S_r, the maximum intensity of radiation is changing as a parabola. The maximum radiation occurs when S is 0.26λ. When $S_r = 0.52\pi$, the graphics is the most regular and the radiation intensity reaches the maximum value.

IV. SYSTEM DESIGNING AND IMPLEMENTATION

According to the above analysis, the design of AGV positioning and guidance system based on active RFID is composed by fixed reader antenna and vehicle-mounted mobile tag. Reader antenna is composed by Dolph-Chebyshev array and flat reflector with 4 fixed antennas as a group, forming the coverage to an area. If the coverage need to be increased, the amount of antenna groups should be increased too. Tags adopt Dolph-Chebyshev antenna array, vertically fixed on AGV in proper position. The center of label antenna and reader antenna are deployed in the same height.

A. Antenna Design

According to the discussion, , the number of antennas is determined as 8. The side lobe level is $SLL = 18$. According to formula (14), electric intensity of eight source Dolph-Chebyshev array is obtained by:

$$E_8 = A_0\omega + A_1\left(4\omega^3 - 3\omega\right) + A_2\left(16\omega^5 - 20\omega^3 + 5\omega\right) \\ + A_3\left(64\omega^7 - 112\omega^5 + 56\omega^3 - 7\omega\right) \quad (17)$$

Through the calculation, the coefficients are:

$$\begin{cases} A_0 = 2.4177 \\ A_1 = 2.1484 \\ A_2 = 1.6764 \\ A_3 = 1.7009 \end{cases} \quad (18)$$

Accordingly, the relative amplitude of the eight antennas are $\{1, 0.99, 1.26, 1.42, 1.42, 1.26, 0.99, 1\}$.

1) Design of Reader Antenna

The reader antenna was fixed on the ground in order to get the best FNBW. Therefore, taking the Dolph-Chebyshev array space in 0.9λ, the height of antenna array is 6.8λ. The distance between the vibrator and flat reflector is S. The radiation directional diagram of flat reflector antenna and the input impedance are quite sensitive to S. When the spacing reduced, the cross coupling enhanced. When spacing increased, the main beam would get wider. According to the previous impact analysis of horizontal reflection, the optimal distance between the antenna array and the flat reflector is 0.26λ.

Plate size has great influence on the gain strengthening in the front direction of the antenna and elimination of the back radiation. Comparing the condition that both height and width of reflection plate are small, it could be observed that when the reflect plate height is small, the front-to-back ratio is still very small. Through experiment and theoretical analysis, the design of the reflection plate is optimized. In the point of economical view, to satisfy the requirements of practical engineering, reflection plate with the height of 9λ and width of 2.5λ is selected.

2) Design of Tag Antenna and System

The tag antenna as an emitter also uses Dolph-Chebyshev array. But the tag antenna needs to be mounted on the AGV while moving frequently. The bigger size antenna will affect the safety of AVG's movement. Therefore, a smaller unit array within spacing of 0.5λ is used with the total height of 4λ. Working in the frequency of 2.45G, the total height of tag antennas is about 0.5m.

Far field active RFID system continuously receives electromagnetic information of active tags to complete positioning and guidance of an AVG. In order to meet the requirements of real-time positioning in a certain speed, the AVG needs to meet certain sending frequency in per unit-time. The average speed of AGV is 2m/s-5m/s in the designed warehouse in our lab. In order to ensure the accuracy and timeliness of positioning, the information emitting frequency of active tags mounted on AGV vehicle is set as 100 times per second. In this case, an AGV sends a message as it runs every 0.02m-0.05m, which ensures the positioning accuracy and timeliness.

B. Layout of Antenna

In combination with the above discussion of antenna design, the directional function of the sending antenna is $F_S(\theta, \varphi)$. of the Dolph-Chebyshev array factor is set as 0.5λ. The directional function of receiving antenna is $F_R(\theta, \varphi)$ with Dolph-Chobyshev array space of 0.9λ. Thus, the sending function is:

$$F_S(\theta, \varphi) = E_8 \cdot E \quad (19)$$

The receiving function is:

$$F_R(\theta, \varphi) = E_8 \cdot E \cdot G_f(\phi) \quad (20)$$

In the process of antenna arranging, center heights of the tag antenna and reader antenna are arranged in the same.

The vertical angle of antenna height is $\theta = \pi/2$. Let the flat reflection $S_r = 0.52\pi$, we can get:

$$F_S(\theta, \varphi) = a_0 + a_1 + a_2 + a_3 \quad (21)$$

$$F_R(\theta, \varphi) = K \cdot (a_0 + a_1 + a_2 + a_3) \quad (22)$$

$K = 2\sqrt{\dfrac{R_{11} + R_L}{R_{11} + R_L - R_{12}}} \cdot \left|\sin\left(0.52\pi \cdot \cos(\phi)\right)\right|$ is the constant.

Assuming $P_{\min}$ is the threshold value of the reader device, it means when energy value detected by receiving antenna is less than $P_{\min}$, the reader device can't read the signals from this active tags. r is the biggest distance in the longitudinal direction of the receiving antenna electromagnetic field. Due to the energy of active tags supplied by AGV, the sending wavelength of the electromagnetic wave λ and energy P_{in} can be determined as constants. G_1 and G_2 are the gains of receiving antenna and transmitting antenna. Therefore, the energy threshold can be obtained by formula (5) when the longest distance r is determined. We can get:

$$P_{min} = \frac{\lambda^2 G_1 G_2 F_S^2(\theta,\varphi) F_R^2(\theta,\varphi) P_{in}}{(4\pi r)^2} \qquad (23)$$

According to the maximum coverage of active RFID, the longest distance along the vertical direction of the antenna coverage field will be $r = 20$. Using formula (24) with $\varphi \in [-\pi, \pi]$ and P_{min}, the coverage of electromagnetic field is [-32m,+32m]. For ensuring the electromagnetic fields coverage, the horizontal distance between an antenna and another antenna is set as 5m. So when an AGV runs in the antenna group, the tags' signal can be detected at least by four antennas. Since the farthest longitudinal radiation distance is 20m, the distance between antennas in the longitudinal direction of the electromagnetic field is 19m.

Fig. 9 shows the coverage of four sets of antennas which have certain blind spots (albeit diminutively). The width d_b of the shadow of the blind area in Fig 9 (a) is 1m. Therefore, after the position of the antenna is determined, a channel needs to be limited. Fig. 10 (a) shows the channel in the shadow area covered by two thick lines.
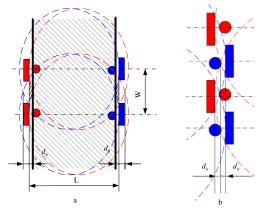

Fig. 9 Blind area of antenna coverage and overlapping

For the vertical overlap area, d_s is the distance between the two antenna groups and let $d_s = 2d_b$ as shown in Fig. 10 (b). A blind area is just completely covered by two crossed antenna groups. Therefore, through the antenna arranged alternately, AVG can be located in the whole area.

C. AGV Positioning

Substituting the receiving function (23) and sending function (22) into the Friis transmission formula, we can get:

$$P_{re}(\theta,\varphi) = K' \cdot \frac{\sin(0.52\pi \cdot \cos\varphi)}{r^2} \qquad (24)$$

$K' = 2 \cdot \left[\frac{\lambda}{4\pi}\right]^2 G_1 G_2 (a_0 + a_1 + a_2 + a_3)^2 \sqrt{\frac{R_{11} + R_L}{R_{11} + R_L - R_{12}}} P_{in}$ is the constant. So the Friis transmission formula only relates to φ and r. Let the detection coordinates of AGV is (x, y). Through coordinate system transforming, φ and r can be replaced by x and y in the Friis transmission as shown in Fig. 10.
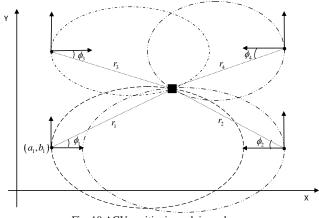

Fig. 10 AGV positioning solving scheme

From Fig. 10, coordinate of No. 1 antenna is (a_1, b_1). The active tag polar coordinate relative to No. 1 antenna could be expressed as $(r_1 \cos\varphi_1, r_1 \sin\varphi_1)$. The coordinate of No. 2 antenna is (a_2, b_2) with its active tag polar coordinate relative $(r_2 \cos\varphi_2, r_2 \sin\varphi_2)$. Thus, we can get:

$$\cos\varphi_1 = \frac{x_1}{\sqrt{x_1^2 + y_1^2}} = \frac{x - a_1}{\sqrt{(x-a_1)^2 + (y-b_1)^2}} \qquad (25)$$

$$r_1 = \sqrt{(x-a_1)^2 + (y-b_1)^2} \qquad (26)$$

The Friis equation of No. 1 antenna is

$$P_1(r,\varphi) = \frac{K \sin\left(0.52\pi \cdot \frac{x - a_1}{\sqrt{(x-a_1)^2 + (y-b_1)^2}}\right)}{(x-a_1)^2 + (y-b_1)^2} \qquad (27)$$

The Friis equation of No. 2 antenna is

$$P_2(r,\varphi) = \frac{K \sin\left(0.52\pi \cdot \frac{a_2 - x}{\sqrt{(x-a_2)^2 + (y-b_2)^2}}\right)}{(x-a_2)^2 + (y-b_2)^2} \qquad (28)$$

From Fig. 10, solving the simultaneous FriiS equations of antenna No.1 and No.2, two points of intersection can be obtained. By the same token, two points of intersection can be obtained by the simultaneous FriiS equations of antenna No.1 and No.3. It ensures that the signal could be detected effectively by at least four antennas. If this amount is more than four, then four antennas with stronger field intensity will be chosen.

D. Simulation and System Implementation

1) Simulation Result

In order to verify the approaches proposed in this paper, simulation experiment is carried out in windows XP operating system and the environment of MATLAB2009a. Walking speed of the AGV is 2m/s. Sending frequency of the signal is 200times/s. The precision value of inflection point is 0.07m. The accuracy value of endpoint is 0.05m. The path width is 0.lm. The perturbation error is set as 1% - 2%.
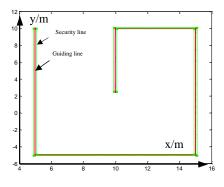
Fig. 11 Simulative path

Fig. 11 shows a complete AGV moving path. In this figure, green border is the security cordon. An AGV acts in green frame is a safe. Red border is the initial path guidance line. According to the diagram, AGV positioning and navigation through the far field active RFID system, the getting out of the security cordon never happens in the running process.
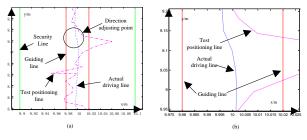

Fig. 12 Simulative movement of AGV

Fig. 12 is the partial enlargement of the simulate image. AGV is in moving state. The pink line is AGV location calculated by the active far-field RFID positioning system. The blue line is the actual path of AGV. It can be clearly seen in the picture that there are some disturbances between the position measured by the antenna group and the actual path of AGV. However, the AGV has strong resilience on the disturbances. As is shown in the marked area in Fig. 12, it can be found after amplification, AGV merely reorient several times in the process of driving.
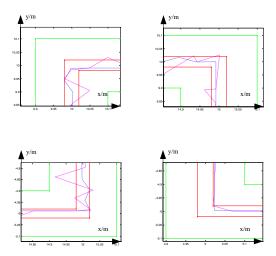

Fig. 13 Simulative turning sketch AGV

Fig. 13 is a partial view of four turning parts. In order to

ensure smoothness, turning point is slightly weakened, it can be seen from the graph, no complex positioning process occurs in the turning process. After entering the neighborhood of turning point, a new path is generated according to the break point and the target point to ensure the accuracy of the direction of travelling AGV.
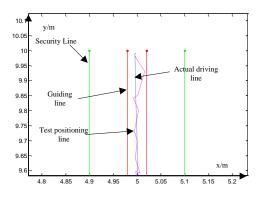

Fig. 14 Simulation of terminal location sketch of AGV

Fig. 14 is the partial view of the end portion. It can be seen in the graph, AGV is relatively stable in the final movement. For AGV path simulation, three paths are formed. First one is planning path, which is determined by the starting point and end point. Second one is testing path. An AGV transmits in the operation process and the testing path is obtained by positioning of antenna. The third one is the actual path. Ten points are selected to present the simulation results as shown in Table 5. The target endpoint (X_r, Y_r) is recorded by the coordinates of the simulated path. the testing path coordinate is (X_a, Y_a), and the actual path coordinate is (X_a, Y_a).

Table. 5 Coordinate data of AGV moving process (m)

	1	2	3	4	5	6	7	8	9	10	Last
X_t	10.00	10.00	14.96	15.00	15.00	15.00	10.06	5.05	5.00	5.00	5.00
Y_t	4.95	9.92	10.00	5.10	0.09	-4.90	-5.00	-5.00	-0.03	4.96	10.00
X_a	10.00	10.01	14.96	14.99	15.01	14.99	10.06	5.05	5.00	5.01	5.00
Y_a	4.95	9.92	9.93	5.10	0.09	-4.90	-4.98	-4.99	-0.03	4.96	9.97
X_r	10.00	10.00	14.95	15.00	15.00	15.00	10.05	5.05	5.00	5.00	5.01
Y_r	4.95	9.95	9.99	5.09	0.09	-4.90	-4.98	-4.99	-0.03	4.97	9.97

The difference between testing path and the simulated path is defined as Δ_f (movement error). The difference between the test path and actual path is Δ_e (measurement error). Table 6 shows the statistics analysis of Δ_f .and Δ_e .

Table. 6 Statistics of movement error and measurement error (m)

	1	2	3	4	5	6	7	8	9	10	Last	Avg.
Δ_f	0.00	0.01	0.07	0.01	0.01	0.01	0.02	0.01	0.00	0.01	0.03	0.016
Δ_e	0.00	0.03	0.01	0.01	0.00	0.00	0.02	0.01	0.00	0.01	0.03	0.012

According to the Table 6, the average movement error and measurement error are $\Delta_f = 0.016$ m and $\Delta_e = 0.012$ m respectively. It could be concluded that the far-field active RFID system positioning accuracy is higher. The movement is more stable and the fluctuating rate is smaller.
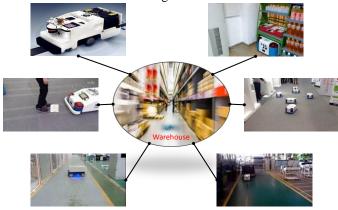

Fig. 15 System implementation in a laboratory warehouse

2) System Implementation

Fig. 15 presents a real-life system implementation in a laboratory warehouse which covers area of 20 m^2. Five AGVs labeled as No. 1 to No. 5 are deployed in the warehouse. Four antennas are deployed on each corner and two antennas are deployed on the ceiling so that the signals are able to cover all the areas, where 4 antennas with stronger field strength are chosen to determine the AGV locations. Table 7 shows the system testing results comparing the set 10 points and actual coordinates with a travelling path of No.2 AGV. Q means the quantities of AGV and P means the points. The coordinates of 10 points are (0, -1), (0, -0.8), (0, -0.6), (0, -0.4), (0, -0.2), (1, 0), (2, 0), (3, 0), (4, 0), and (5, 0).

Table. 7 System Testing Results

P \ Q	1	2	3	4	5
1	(0, -1)	(0, -1)	(0, -1)	(0, -1)	(0, -1)
2	(0.05, -0.83)	(0.05, -0.85)	(0.04, -0.80)	(0.07, -0.80)	(0.07, -0.88)
3	(0.06, -0.67)	(0.08, -0.69)	(0.06, -0.77)	(0.07, -0.77)	(0.05, -0.77)
4	(0.05, -0.38)	(0.05, -0.38)	(0.06, -0.40)	(0.04, -0.44)	(0.04, -0.48)
5	(0.06, -0.24)	(0.06, -0.20)	(0.05, -0.28)	(0.05, -0.34)	(0.05, -0.24)
6	(0.85, 0.03)	(0.85, 0.02)	(0.83, 0.02)	(0.90, 0.04)	(0.78, 0.03)
7	(1.98, 0.04)	(1.88, 0.04)	(1.90, 0.04)	(1.90, 0.07)	(1.91, 0.07)
8	(3.02, 0.04)	(3.01, 0.04)	(2.98, 0.03)	(3.00, 0.06)	(2.85, 0.04)
9	(4.00, 0.02)	(4.01, 0.01)	(4.03, 0.03)	(4.08, 0.08)	(4.10, 0.05)
10	(5.00, 0.02)	(5.08, 0.02)	(5.00, 0.02)	(5.10, 0.01)	(4.95, 0.02)

From Table 7, it could be observed that the proposed locating approach is capable of enabling the positioning and navigating AGVs in the warehouse. As the increasing of AGV quantities in the testing environment, the accuracy slightly reduces. That because the signals will be influenced by the AGVs which are moving closely. However, in a larger area like in real-life warehouse, the influences will be greatly reduced since an AGV may have more space to move around. It is also observed that the accuracy will be greatly reduced after an AGV passing a quarter bend. The control service for the bending movement attributes to the accuracy reduction, thus, a more suitable control algorithm with parallel processing capacity is needed to improve this.

V. SUMMARY

This paper introduces an active RFID tag-enabled localization approach for AGV by making full use of magnetic field lines. This approach uses the concept of errors suppression positioning that is used to measure the vertical and horizontal reflection of suppressions. The positioning system for AGV is presented in terms of design of antenna and positioning manner. The implementation and simulation are illustrated.

Several contributions are significant. First, Dolph-Chebyshev antenna array is used in this system to enable AGV with more precise location implementation. The magnetic field lines are used for precise positioning. Secondly, this system is proved to be feasible and practical in real-life implementation after simulation tests. It is observed that the far-field active RFID system positioning accuracy is higher, the move is more stable and the fluctuating rate is smaller.

The future work will be carried out as follows. First of all, the accurate of positioning information will be used for advanced decision-makings like route optimization so that the cost could be reduced. In this case, new mathematic models are needed. Secondly, the real-life application of this system in warehouse management system or logistics control will be carried out to verify the feasibility and practicality in real-life applications.

REFERENCES

[1] N. Q. Wu and M. C. Zhou, "Modeling and deadlock control of automated guided vehicle systems," *Mechatronics, IEEE/ASME Transactions on,* vol. 9, pp. 50-57, 2004.

[2] B. Kehoe, S. Patil, P. Abbeel, and K. Goldberg, "A survey of research on cloud robotics and automation," *Automation Science and Engineering, IEEE Transactions on,* vol. 12, pp. 398-409, 2015.

[3] S. Lee, K. C. Lee, M. H. Lee, and F. Harashima, "Integration of mobile vehicles for automated material handling using Profibus and IEEE 802.11 networks," *Industrial Electronics, IEEE Transactions on,* vol. 49, pp. 693-701, 2002.

[4] D. Y. Lee and F. DiCesare, "Integrated scheduling of flexible manufacturing systems employing automated guided vehicles," *Industrial Electronics, IEEE Transactions on,* vol. 41, pp. 602-610, 1994.

[5] J. Zhao, W. Wang, K. Sun, and Y. Liu, "A Bayesian Networks Structure Learning and Reasoning-Based Byproduct Gas Scheduling in Steel Industry," *Automation Science and Engineering, IEEE Transactions on,* vol. 11, pp. 1149-1154, 2014.

[6] R. Y. Zhong, G. Q. Huang, S. L. Lan, Q. Y. Dai, C. Xu, and T. Zhang, "A Big Data Approach for Logistics Trajectory Discovery from RFID-enabled Production Data," *International Journal of Production Economics,* vol. 165, pp. 260-272, 2015.

[7] L. Wang, L. Da Xu, Z. Bi, and Y. Xu, "Data cleaning for RFID and WSN integration," *Industrial Informatics, IEEE Transactions on,* vol. 10, pp. 408-418, 2014.

[8] M. Y. Ahmad and A. S. Mohan, "Novel bridge-loop reader for positioning with HF RFID under sparse tag grid," *Industrial Electronics, IEEE Transactions on,* vol. 61, pp. 555-566, 2014.

[9] R. Y. Zhong, Q. Dai, T. Qu, G. Hu, and G. Q. Huang, "RFID-enabled real-time manufacturing execution system for mass-customization production," *Robotics and Computer-Integrated Manufacturing,* vol. 29, pp. 283-292, 2013.

[10] H.-T. Hsu and T.-J. Huang, "A koch-shaped log-periodic dipole array (LPDA) antenna for universal ultra-high-frequency (UHF) radio frequency identification (RFID) handheld reader," *Antennas and Propagation, IEEE Transactions on,* vol. 61, pp. 4852-4856, 2013.

[11] S. Makris, G. Michalos, and G. Chryssolouris, "RFID driven robotic assembly for random mix manufacturing," *Robotics and Computer-Integrated Manufacturing,* vol. 28, pp. 359-365, 2012.

[12] E. Vahedi, R. K. Ward, and I. F. Blake, "Performance analysis of RFID protocols: CDMA versus the standard EPC Gen-2," *Automation Science and Engineering, IEEE Transactions on,* vol. 11, pp. 1250-1261, 2014.

[13] W.-T. Chen, "An accurate tag estimate method for improving the performance of an RFID anticollision algorithm based on dynamic frame length ALOHA," *Automation Science and Engineering, IEEE Transactions on,* vol. 6, pp. 9-15, 2009.

[14] M. Kim and N. Y. Chong, "Direction sensing RFID reader for mobile robot navigation," *Automation Science and Engineering, IEEE Transactions on,* vol. 6, pp. 44-54, 2009.

[15] W. Zhu, J. Cao, Y. Xu, L. Yang, and J. Kong, "Fault-tolerant RFID reader localization based on passive RFID tags," *Parallel and Distributed Systems, IEEE Transactions on,* vol. 25, pp. 2065-2076, 2014.

[16] A. Lehto, J. Nummela, L. Ukkonen, L. Sydänheimo, and M. Kivikoski, "Passive UHF RFID in paper industry: Challenges, benefits and the application environment," *Automation Science and Engineering, IEEE Transactions on,* vol. 6, pp. 66-79, 2009.

[17] N. Decarli, F. Guidi, and D. Dardari, "A novel joint RFID and radar sensor network for passive localization: Design and performance bounds," *Selected Topics in Signal Processing, IEEE Journal of,* vol. 8, pp. 80-95, 2014.

[18] K. Sato and Y. Sano, "Practical and intuitive controller design method for precision positioning of a pneumatic cylinder actuator stage," *Precision Engineering,* vol. 38, pp. 703-710, 2014.

[19] K.-A. Lee and K.-C. Ko, "Propagation Model of High-Power Electromagnetic Pulse by Using a Serial–Parallel Resistors Circuit," *Plasma Science, IEEE Transactions on,* vol. 42, pp. 3309-3312, 2014.

[20] S. A. Mirbozorgi, H. R. Bahrami, M. Sawan, and B. Gosselin, "A smart multicoil inductively coupled array for wireless power transmission," *Industrial Electronics, IEEE Transactions on,* vol. 61, pp. 6061-6070, 2014.

[21] H. Zhang, Y. Shi, and J. Wang, "On energy-to-peak filtering for nonuniformly sampled nonlinear systems: a Markovian jump system approach," *Fuzzy Systems, IEEE Transactions on,* vol. 22, pp. 212-222, 2014.

[22] M. V. Bueno-Delgado, R. Ferrero, F. Gandino, P. Pavon-Marino, and M. Rebaudengo, "A geometric distribution reader anti-collision protocol for RFID dense reader environments," *Automation Science and Engineering, IEEE Transactions on,* vol. 10, pp. 296-306, 2013.

[23] E. DiGiampaolo and F. Martinelli, "Mobile robot localization using the phase of passive UHF RFID signals," *Industrial Electronics, IEEE Transactions on,* vol. 61, pp. 365-376, 2014.

[24] D. Wang, J. Hu, and H.-Z. Tan, "A Highly Stable and Reliable 13.56-MHz RFID Tag IC for Contactless Payment," *Industrial Electronics, IEEE Transactions on,* vol. 62, pp. 545-554, 2015.

Shaoping Lu received the B.Eng. degree in mechanical manufacturing and automation and the M.Eng. Degree in industrial engineering from the Huazhong University of Science and Technology, Wuhan, China, in 1982 and 2000 respectively, and the Ph.D. degree in control theory and control engineering from Shandong University, Shandong, in 2011.

Dr. Lu holds the position of the vice director of the Supply Chain Collaborative Innovation Center of Shenzhen University, the director of Transport and Logistics Department in Shenzhen University, and the director of Modern Logistics Laboratory in Shenzhen University. From 1994 to 1998, he was a senior engineer in the New Technology Research Center of Shenzhen University. From 1992 to 1994, he was a senior programmer and system engineer of the International Software Development (Shenzhen) Co.,Ltd. From 1982 to 1992, he had been taken the position of an engineer, manager etc. of Jianghan Oil Management Board in Qianjiang, Hubei.

Dr. Lu is also the council member of China Society of Logistics (since 2005), and Guangdong Society of Supply Chain (since 2015).

Chen Xu received the B.Sc. and M.Sc. degrees from Xidian University, China in 1986 and 1989, respectively, and the Ph.D. degree from Xi'an Jiaotong University, China, in 1992.

He joined the Shenzhen University, Shenzhen, China in 1992 and currently is a Professor. From September 1999 to January 2000, he was a research fellow with the Kansai University, Japan. From August 2002 to August 2003, he was a research fellow with the University of Hawaii, USA. At present, Dr. Xu is the member of College Mathematic Teaching Guiding Committee of the Ministry of Education, vice chairman of the Guangdong Society for Industrial and Applied Mathematics, vice director of Guangdong Mathematic Teaching Guidance Committee.

His research interests are wavelet analysis, intelligent computing, image processing, intricate network and modern logistics.

Ray Y. Zhong (M'13) received the Ph.D. degree in industrial and manufacturing systems engineering from the University of Hong Kong, China, in 2013, M.S. degree in signal and information processing from Guangdong University of Technology, China, in 2009 and B.S. degree in mathematics and computer science and technology from Gannan Normal University, China, in 2004.

Dr. Zhong is current a lecturer at Department of Mechanical Engineering, The University of Auckland. From June 2013 to December 2015, he is a Post-doctoral Fellow with the Department of Industrial and Manufacturing Systems Engineering, The University of Hong Kong. His research interest includes Big Data in manufacturing and service, Advanced Planning and Scheduling, and RFID in Internet of Manufacturing Things.

Dr. Zhong is member of LSCM HK, IET, ASME, IIE, and IEEE. He was a recipient of the Best Conference Paper Award in the 2014 IEEE International Conference on Networking, Sensing and Control (ICNSC14) and Certificate of Merit in the Hong Kong U-21 RFID Awards 2011, GS1 HK.